PHYSICAL REVIEW B VOLUME 27, NUMBER 8 15 APRIL 1983

Scattering-theoretical method for relaxed and reconstructed surfaces with applications to GaAs(110) and Si(100)-(2×1)

M. Schmeits
Institut de Physique, Université de Liège, Sart-Tilman, B-4000 Liège, Belgium

A. Mazur and J. Pollmann
Institut für Physik, Universität Dortmund, D-4600 Dortmund 50, Federal Republic of Germany
(Received 6 July 1982)

The tight-binding scattering-theoretical method for the calculation of electronic properties of *relaxed* and *reconstructed* surfaces is described in detail and applied to the relaxed GaAs(110) surface and the reconstructed Si(100)-(2×1) surface. For the underlying bulk electronic structure, we employ realistic empirical tight-binding Hamiltonians retaining first- and second-nearest-neighbor interactions. In our calculations we have used surface-structural models, proposed in the literature on the basis of total energy minimization calculations. These models are in good agreement with low-energy electron-diffraction data. Relaxation- and reconstruction-induced changes in the interaction matrix elements with interatomic distance d are taken into account by the d^{-2} scaling law, as proposed by Harrison. We discuss our results in terms of surface band structures and wave-vector—integrated as well as wave-vector—resolved layer densities of states. These theoretical data allow for a detailed discussion of the origin and physical nature of the surface-induced features. In particular, the effects of relaxation or reconstruction on the ideal surface electronic properties can transparently be analyzed in the framework of the current method. Comparison of our results with both angle-integrated and angle-resolved photoemission data shows very good agreement confirming the charge-transfer bond-angle relaxation model for GaAs(110) and the asymmetric dimer model for Si(100)-(2×1).

I. INTRODUCTION

The electronic structure of semiconductor surfaces has become a subject of large theoretical and experimental activity during the past decade. This is due to both the intrinsic fundamental interest in the problem and to the practical relevance of the subject. Nevertheless, bulk electronic properties of crystals continue to be much better understood than surface electronic properties. This is related to both experimental and theoretical reasons. For the theorist, a surface introduces two new complications as compared to the bulk electronic structure problem: First, there is the lack of periodicity perpendicular to the surface plane and second, there occurs a rearrangement of atoms in the outermost layers near the surface. These structural changes are referred to as relaxation or reconstruction, depending on whether the movement of the atoms leads to a symmetry change of the surface unit cell or not. Until now, the surface-layer atom positions cannot be determined with the same accuracy as for bulk atoms, because there exists no experimental method for surface-structure determination which is equivalent to the standard bulk techniques. Low-energy electron diffraction (LEED) readily yields the translational symmetry of the surface layer and the orientation of the surface unit mesh with respect to the underlying bulk structure but it does not directly reveal atomic positions within the unit cell.

For the determination of the surface atomic coordinates two complementary approaches are used currently which are both based on joint theoretical and experimental studies. One is LEED combined with dynamical diffraction theory, which has been applied to a large number of semiconductor surfaces. The other is angle-resolved photoelectron spectroscopy together with surface electronic structure theory. For certain assumed structural models the calculated electronic structure is compared to the angle-resolved ultraviolet photoelectron spectroscopy (ARUPS) data in order to either confirm or rule out the chosen structural model. A precise knowledge of the electronic structure, therefore, is very helpful for determining the relaxation or reconstruction behavior of a given surface.

Many different theoretical methods are currently used to study electronic properties of surfaces: the cluster, slab, superlattice, matching, transfer-matrix or scattering-theoretical methods. For the details of these methods, we refer the reader to Refs. 1—14, together with the included references. The scattering-theoretical method has been applied successfully to the study of ideal surfaces[1] and relaxed surfaces.[15–17]

In the present paper we describe in detail the formal extensions of the scattering-theoretical method necessary for the treatment of relaxed or reconstructed surfaces and present some applications of the formalism. As examples, we have chosen surfaces which have gained much interest in the past, namely the relaxed GaAs(110) surface and the reconstructed Si(100)-(2×1) surface. This allows for comparison of our results with experimental data and with theoretical results obtained by other methods. Despite the large amount of both theoretical and experimental information on these surfaces, they still remain a subject of current interest, showing that the detailed electronic structure has not yet reached a state of common agreement.

In the scattering-theoretical method (STM) a surface is treated as a localized perturbation of a bulk solid. The bulk crystal is described by an empirical tight-binding Hamiltonian. In the examples we present, second-nearest-neighbor interactions are included in the bulk Hamiltonians, leading to a realistic bulk electronic structure, at least for the occupied states. The ideal surface is then created by removing two layers of atoms (since second-nearest-neighbor interactions are included) so that two semi-infinite decoupled crystals result. In addition, the necessary changes of the tight-binding matrix elements of the relaxed or reconstructed surface are taken into account by an empirical scaling of the interactions with interatomic distances. The modifications of the directions and the distances between the atoms in the surface layers give rise to pronounced changes in the surface electronic structure of relaxed and reconstructed surfaces as compared to ideal surfaces. On the basis of the present formalism we have studied these changes by calculating the new bound-state energy-level positions and wave-vector—resolved layer densities of states. An analysis of the latter allows for a detailed investigation of the relaxation- or reconstruction-induced shifts of state-density peaks within the projected bulk band continua.

The scattering-theoretical method has several virtues:

(a) Starting from a realistic empirical tight-binding bulk Hamiltonian we arrive at results for the surface electronic structure of real semi-infinite solids, which are quantitatively meaningful. They do not only allow us to discuss general physical trends but they can also be compared successfully with experimental data.

(b) The bound-state energies and the wave-vector—resolved densities of states can directly be obtained, once the bulk Hamiltonian and the surface atomic structures are specified. These quantities can be related to experimental data as obtained, e.g., by ARUPS measurements.

(c) The expensive part of the calculations (i.e., the setup of the bulk Green's function in a layer-orbital representation) needs to be done only once, when different structural models are to be investigated. A large amount of useful information is obtained by a modest numerical effort. The STM is thus a very efficient and fast approach for the study of electronic properties of surfaces with high spectral resolution.

This paper is organized as follows: In Sec. II we develop the general theory for the treatment of relaxed or reconstructed surfaces within the Green's function approach. In Sec. III we apply the formalism to a relaxed surface and discuss the electronic structure of ideal and relaxed GaAs(110). Section IV is devoted to the study of the reconstructed Si(100)-(2×1) surface. A short summary in Sec. V concludes the paper.

II. SCATTERING-THEORETICAL METHOD FOR RELAXED AND RECONSTRUCTED SURFACES

The determination of the electronic structure of *ideal* surfaces using the scattering-theoretical method has been described in detail in Ref. 1. In order to establish the nomenclature, we briefly recall the basic equations for the general formalism and its application to ideal surfaces before discussing the cases of relaxed and reconstructed surfaces in some detail.

A. General formalism

In the scattering-theoretical method surfaces are treated as localized perturbations of a perfect, three-dimensionally periodic bulk solid. The perturbation U that creates a surface is two-dimensionally periodic parallel to the surface and highly localized perpendicular to the surface.

The unperturbed bulk solid is described by an effective one-electron Hamiltonian H_b. The bulk band structure and the corresponding eigenstates are obtained by solving the Schrödinger equation:

$$H_b \mid n,\vec{k}\rangle = E_n(\vec{k}) \mid n,\vec{k}\rangle, \tag{1}$$

where n is the band index and $\vec{k}$ is the Bloch wave vector. The bulk Green's function G_b is defined as

$$G_b(E)=\lim_{\epsilon\to 0^+}(E+i\epsilon-H_b)^{-1} =:(E^+-H_b)^{-1} \quad (2)$$

and the bulk density of states (DOS) is given by

$$N_b(E)=-\pi^{-1}\mathrm{Tr}\,\mathrm{Im}G_b(E)\ . \quad (3)$$

The Hamiltonian of a crystal with two surfaces which are infinitely far apart from one another is given by

$$H_s=H_b+U_s \quad (4)$$

where U_s formally describes the creation of the surfaces. The specific form of U_s is, of course, different for ideal, relaxed, or reconstructed surfaces and will be given below. It should be noted that it is only the localized perturbation U_s that changes for the different types of surfaces. The main part of H_s, namely H_b, is unaffected thereby.

The Green's function of the perturbed system H_s, i.e., of a crystal with two surfaces infinitely far apart from one another, is determined by the Dyson equation,

$$G_s(E)=G_b(E)+G_b(E)U_sG_s(E)\ . \quad (5)$$

The formal solution for $G_s(E)$ is given by

$$G_s(E)=G_b(E)+G_b(E)T_s(E)G_b(E) \quad (6)$$

in terms of the bulk Green's function $G_b(E)$ and the surface scattering matrix

$$T_s(E)=U_s[1-G_b(E)U_s]^{-1}\ . \quad (7)$$

Scattering of bulk eigenstates at the surface can give rise to bound surface states or resonances (antiresonances). The bound surface states are determined by the poles of the surface scattering matrix, i.e., by the solution of

$$D(E)=0\ , \quad (8)$$

where

$$D(E)=\det||1-G_b(E)U_s||\ . \quad (9)$$

Resonances and antiresonances induce increases or decreases in the unperturbed (i.e., bulk) density of states, respectively. They can be identified by calculating the total change in the density of states,

$$\Delta N(E)=\pi^{-1}\mathrm{Tr}\,\mathrm{Im}[G_s(E)-G_b(E)] =-\pi^{-1}d\phi(E)/dE\ , \quad (10)$$

where the phase shift $\phi(E)$ is defined as

$$\phi(E)=\arg D(E)\ . \quad (11)$$

The localization properties of bound states as well as resonances can be obtained from the layer densities of states (LDOS). They are obtained by taking partial traces of the imaginary part of $G_s(E)$ in a layer-orbital representation.

B. Linear combination of atomic orbitals representation

In order to apply the general formalism, we need an explicit representation of H_s, H_b, U_s, and the corresponding Green's functions. We use an orthonormal set of localized orbitals $\varphi_\alpha(\vec{r})$ to expand the wave functions. Symmetry-adapted linear combinations thereof are used to represent the operators.

In $\vec{r}$ representation, the bulk wave functions $\psi_{n,\vec{k}}(\vec{r})=\langle\vec{r}\mid n,\vec{k}\rangle$ are expanded as follows:

$$\psi_{n,\vec{k}}(\vec{r})=\sum_{\alpha,\nu}C^n_{\alpha\nu}(\vec{k})\chi^{\alpha\nu}_{\vec{k}}(\vec{r}), \quad (12)$$

with

$$\chi^{\alpha\nu}_{\vec{k}}(\vec{r})=\frac{1}{\sqrt{N_3}}\sum_j e^{i\vec{k}\cdot(\vec{R}_j+\vec{\tau}_\nu)}\varphi_\alpha(\vec{r}-\vec{R}_j-\vec{\tau}_\nu) \quad (13)$$

where $\vec{R}_j$ is a Bravais-lattice vector and $\vec{\tau}_\nu$ specifies the positions of the atoms in the unit cell. N_3 is the number of lattice points in the normalization volume of the bulk lattice. For semiconductors like Si, Ge, or GaAs the set of localized orbitals is usually restricted to atomic s and p functions since these orbitals are mainly involved in the chemical bonding of the materials. For the bulk description, we use the empirical tight-binding method (ETBM) as introduced by Slater and Koster.[18] In this approach, the bulk Hamiltonian matrix elements

$$\langle\varphi_\alpha(\vec{r})\mid H_b\mid\varphi_\beta(\vec{r}-\vec{R}_j-\vec{\tau}_\nu\rangle$$

are treated as parameters. They are chosen such that the resulting ETBM band structure $E_n(\vec{k})$ optimally fits the results of more sophisticated, self-consistent bulk band-structure calculations or experimental ultraviolet photoelectron spectroscopy (UPS) and reflectivity data, or both.

When only a finite number of atomic orbitals per site is taken into account (s, p_x, p_y, and p_z, in our case) this approach has the great advantage that the solution of Eq. (1) is reduced to diagonalizing small matrices (typically 8×8 in size). When only first- and second-nearest-neighbor interactions are retained in the bulk Hamiltonian matrix, the surface-creating perturbation U_s is small in size and the mathematical operations involved in the calculation of bound surface states and resonances [Eqs.

(5)–(11)] can easily be done on a computer.

A natural basis set for surface calculations, which completely exploits the translational symmetry, is the layer-orbital basis. A surface retains a translational symmetry parallel to the surface plane, so that a two-dimensional Bloch wave vector $\vec{q}$ can be introduced to classify the eigensolutions of the system. Layer-orbitals are then given in $\vec{r}$ representation by

$$\langle \vec{r} \mid m,\alpha,\mu;\vec{q} \rangle = \frac{1}{\sqrt{N_2}} \sum_l e^{i\vec{q}\cdot(\vec{\rho}_l + \vec{\lambda}_\mu^m)} \times \varphi_\alpha(\vec{r} - \vec{\rho}_l - \vec{\lambda}_\mu^m) . \tag{14}$$

The number of Bravais-lattice points per layer normalization area is N_2; m labels layers, $\vec{\rho}_l$ are the lattice vectors of the two-dimensional Bravais lattice, and $\vec{\lambda}_\mu^m$ are the positions of the atoms in the unit cell. This vector can be decomposed into a surface-parallel component $\vec{\sigma}_\mu^m$ and a perpendicular component $\vec{\kappa}^m$, which specifies the distance of layer m from the origin, such that

$$\vec{\lambda}_\mu^m = \vec{\sigma}_\mu^m + \vec{\kappa}^\mu . \tag{15}$$

Thus both sets of vectors $\{\vec{\rho}_l, \vec{\lambda}_\mu^m\}$ and $\{\vec{R}_j, \vec{\tau}_\nu\}$ span the entire bulk lattice.

The bulk Bloch wave vector $\vec{k}$ can be decomposed accordingly into a surface-parallel component $\vec{q}+\vec{g}$ and a surface-perpendicular component $\vec{k}_\perp$ as

$$\vec{k} = \vec{q} + \vec{g} + \vec{k}_\perp , \tag{16}$$

where $\vec{g}$ is a reciprocal-lattice vector of the two-dimensional net. Since $\vec{k}$ is restricted to the first bulk Brillouin zone, $\vec{q}+\vec{g}$ is also restricted to the same Brillouin zone.

We are now prepared to represent the operators in Eqs. (2)–(11) in the layer-orbital basis. Since the surface perturbation U_s is different for the different types of surfaces we will discuss its representation separately. The bulk Green's function $G_b(E)$ is, of course, the same in all cases.

Introducing a collective index $l=(m,\alpha,\mu)$, the bulk Green's function is given in the layer-orbital representation by

$$G_{l,l'}^b(\vec{q},E) = \sum_{n,\vec{k}} \frac{\langle l;\vec{q} \mid n\vec{k} \rangle \langle n\vec{k} \mid l';\vec{q} \rangle}{E^+ - E_n(\vec{k})} \tag{17}$$

which reduces to[1]

$$G_{l,l'}^b(\vec{q},E) = \frac{N_2}{N_3} \sum_{\vec{k}_\perp} {\sum_{\vec{g}}}' e^{i\vec{k}_\perp\cdot(\vec{\kappa}^m - \vec{\kappa}^{m'})} e^{i\vec{g}\cdot(\vec{\sigma}_\mu^m - \vec{\sigma}_{\mu'}^{m'})} \times \sum_n \frac{C_l^n(\vec{q}+\vec{g},\vec{k}_\perp) C_{l'}^{n\,*}(\vec{q}+\vec{g},\vec{k}_\perp)}{E^+ - E_n(\vec{q}+\vec{g},\vec{k}_\perp)} . \tag{18}$$

The sum over $\vec{g}$ involves only those $\vec{g}$ vectors for which $\vec{k} = \vec{q}+\vec{g}+\vec{k}_\perp$ lies inside the first bulk Brillouin zone. This sum can always be eliminated by employing bulk symmetry properties,[1] yielding the final expression

$$G_{l,l'}^b(\vec{q},E) = \frac{L_\perp N_2}{2\pi N_3} \int_{-x_1}^{x_1} dk_\perp e^{i\vec{k}_\perp\cdot(\vec{\kappa}^m - \vec{\kappa}^{m'})} \times \sum_n \frac{C_l^n(\vec{q},\vec{k}_\perp) C_{l'}^{n\,*}(\vec{q},\vec{k}_\perp)}{E^+ - E_n(\vec{q},\vec{k}_\perp)} , \tag{19}$$

where $L_\perp$ is the length of the normalization volume perpendicular to the surface. The $k_\perp$-integration interval $-x_1$ to x_1 depends on the particular surface considered[1]; e.g., for a (100) surface of a diamond-type lattice, x_1 is equal to $2\pi/a$.

C. Ideal surfaces

For the study of the electronic structure of ideal surfaces, a perturbation $U_s^{\rm id}$ is introduced which "removes" sufficiently many layers from the bulk crystal to completely decouple the two resulting surfaces. The removal is accomplished by shifting the on-site matrix elements on all atoms to be removed to infinity.[1] The corresponding surface-creating perturbation $U_s^{\rm id}$ is given by

$$\langle l;\vec{q} \mid U_s^{\rm id} \mid l';\vec{q} \rangle = \lim_{u\to\infty} u\delta_{\alpha\alpha'}\delta_{\mu\mu'}\delta_{mm'} \sum_{m''=1}^{N} \delta_{m,m''} \tag{20}$$

in layer-orbital representation. The sum over m'' is restricted to the N layers to be removed. This number is typically one or two, respectively, if the bulk crystal is described by a first- or a first- and second-nearest-neighbor ETBM Hamiltonian. In consequence, the surface-creating U matrix is very small in size, e.g., 16×16 for ideal GaAs(110) when a second-nearest-neighbor bulk Hamiltonian is used with s, p_x, p_y, and p_z orbitals per atom.

The bound states at an ideal surface are given by the solutions of

$$D^{\rm id}(\vec{q},E) = \det'||-G_{l,l'}^b(\vec{q},E)|| = 0 , \tag{21}$$

as can be seen by inserting Eq. (20) in Eqs. (8) and (9) and carrying out the limit u to infinity. The prime at the determinant is meant to indicate that l and l' are restricted to the subspace of the removed layers [see Eq. (20)] Layer-, atom-, and orbital-resolved densities of states are given by

$$N_l^s(\vec{q},E) = -\pi^{-1}{\rm Im}G_{l,l}^s(\vec{q},E), \tag{22}$$

with the surface Green's function calculated from Eq. (6) in the layer-orbital representation (for details see Ref. 1) and $U_s^{\rm id}$ according to Eq. (20).

D. Relaxed surfaces

Surface-structural changes which are induced by movements of atoms in the outermost layers without changing the translational symmetry of the surface system are referred to as surface relaxations. They do not change the surface unit cell and surface Brillouin zone so that the $\vec{q}$ vector ranges over the same area as for the corresponding ideal surface.

The modifications of the atomic positions in the outermost layers, however, give rise to changes in the interaction matrix elements between these atoms and the other atoms of the system. The surface creating perturbation $U_s^{\rm rel}$ thus needs to consist of two contributions: one which creates an ideal surface and a second part which simultaneously takes into account the relaxation-induced changes. This task is accomplished by the following U matrix:

$$U_s^{\rm rel}=\begin{bmatrix} U_s^{\rm id} & 0 \\ 0 & \mathscr{V}^{\rm rel} \end{bmatrix} . \tag{23}$$

In the layer-orbital representation, the relaxation matrix $\mathscr{V}^{\rm rel}$ reads

$$\langle l;\vec{q}\,|\,\mathscr{V}^{\rm rel}\,|\,l';\vec{q}\,\rangle=\langle l;\vec{q}\,|\,H_s\,|\,l';\vec{q}\,\rangle - \langle l;\vec{q}\,|\,H_b\,|\,l';\vec{q}\,\rangle , \tag{24}$$

and describes the changes of the interaction matrix elements due to relaxation. In the two-center approximation, the Hamiltonian matrix elements between s and p orbitals are given by

$$\langle \varphi_s(\vec{r})\,|\,H\,|\,\varphi_{p_i}(\vec{r}-\vec{\tau})\rangle=\frac{\tau_i}{\tau}V_{sp} ,$$

$$\langle \varphi_i(\vec{r})\,|\,H\,|\,\varphi_{p_j}(\vec{r}-\vec{\tau})\rangle=\frac{\tau_i\tau_j}{\tau^2}\{V_{pp\sigma}-V_{pp\pi}\} +\delta_{ij}V_{pp\pi} \tag{25}$$

with $i,j=x,y,z$. Not only the direction cosines but also the interactions V change when the atomic distances between neighboring atoms are changed. For these changes we employ the empirical scaling law suggested by Harrison,[19] according to which interatomic matrix elements vary as d^{-2} with varying internuclear distance d. This scaling law has also been used with great success by Chadi[6,13] for his studies of relaxed and reconstructed semiconductor surfaces. If V_i^0 are the matrix elements for the ideal crystal, variations with distance are thus included by

$$V_i=V_i^0\left[\frac{d_0}{d}\right]^2 , \tag{26}$$

where d_0 and d are the interatomic distances before and after relaxation, respectively. Equations (25) and (26) show how distance changes as well as angular displacements induced by relaxation are taken into account.

Inserting (24)—(26) in (23) and using the general formalism of Sec. II A, bound states can be calculated from Eq. (8) and layer densities of states are given by Eq. (22) where $U_s^{\rm rel}$ has to be used in the calculation of the surface Green's function. Since $U_s^{\rm id}$ creates two equivalent ideal surfaces, it is computationally most efficient to set up $\mathscr{V}^{\rm rel}$ in such a way that it relaxes only one of the two surfaces. Applying Eq. (22) on both sides of the "surface-creating cut" yields then simultaneously the properties of the relaxed surface and those of the ideal surface (for reference's sake).

E. Reconstructed surfaces

In most of the formalisms for the evaluation of electronic properties of surfaces, a reconstructed surface constitutes an entirely new system as compared to the corresponding ideal surface. This is not the case in the scattering-theoretical method nor is it the case in nature. The reconstruction of a surface can introduce interactions between the eigenstates of the ideal surface system which were symmetry-forbidden at the ideal surface. The symmetry reduction at the reconstructed surface changes the selection rules and thus allows for new interactions previously forbidden. The eigenstates of the ideally terminated semi-infinite solid scatter at the reconstruction-induced surface net. These physical facts become directly apparent in our current formalism.

When a surface reconstructs, the translational symmetry is changed and, therefore, the surface unit cell is modified. The basis vectors of the new unit cell $\vec{b}_i$ are expressed as integer multiples of the old basis vectors $\vec{a}_i$ by

$$\vec{b}_1=\alpha_1\vec{a}_1, \qquad \vec{b}_2=\alpha_2\vec{a}_2, \tag{27}$$

for commensurate reconstructions without rotations being involved; α_1 and α_2 are integers referring to a $\alpha_1\times\alpha_2$ reconstructed surface. If rotations are involved, the vectors $\vec{b}_i$ depend on both $\vec{a}_1$ and $\vec{a}_2$. For the sake of simplicity, we restrict our discussion to the simple case given above, since we will present in this paper only applications to the Si(100)-(2×1) surface as an example. Extensions of the formalism

to more complicated reconstructions are straightforward. The reconstruction introduces a new reciprocal surface lattice whose unit vectors are given by the corresponding ideal surface unit vectors divided by α_1 and α_2, respectively. The new surface Brillouin zone (SBZ) in consequence, covers only an integer fraction of the ideal surface Brillouin zone. The two-dimensional wave vector of the reconstructed SBZ, which we will label $\tilde{\vec{q}}$ for clarity's sake, is thus restricted to an area which is $1/\alpha_1\alpha_2$ smaller than the ideal SBZ. The number of orbitals per layer unit cell increases correspondingly, which merely represents the fact that the total number of electronic states is conserved.

Surface reconstruction is now described in our approach by the following surface perturbation matrix:

$$U_s^{\rm rec}=\begin{pmatrix} U_s^{\rm id} & 0 \\ 0 & \mathscr{V}^{\rm rec} \end{pmatrix}, \tag{28}$$

which is formally similar to the surface relaxation matrix. There is one distinct difference, however, for reconstructed surfaces, as compared to relaxed surfaces. For the representation of $U_s^{\rm rec}$ and the corresponding Green's functions a layer-orbital representation is needed that takes into account the reduced symmetry and is thus *different* from the ideal surface layer-orbital representation. There are thus two distinctly different features to be taken into account. One is the new basis and the other are the explicit effects of $\mathscr{V}^{\rm rec}$. It is interesting to discuss one at a time and to pursue how the formal results change when the new basis is used to represent the operators even without "switching on" the reconstruction-induced interactions in $\mathscr{V}^{\rm rec}$. This is equivalent to studying the electronic structure of an ideal surface using artificially a too large, i.e., the reconstructed unit cell. Such a procedure results in a superposition of electronic properties of the unreconstructed 1×1 surface. The 1×1 electronic structure becomes *backfolded* $\alpha_1\alpha_2$ times onto the reconstructed SBZ. The reconstruction matrix $\mathscr{V}^{\rm rec}$ finally leads to interactions, mixings, and splittings of these backfolded states.

The backfolded ideal surface-electronic structure, therefore, constitutes a valuable intermediate step in the treatment of reconstructed surfaces. As the symmetry-adapted basis, we use (in $\vec{r}$ representation)

$$\langle \vec{r}\,|\,m,\alpha,\epsilon,\tilde{\vec{q}}\,\rangle=\frac{1}{\sqrt{N_2^r}}\sum_l e^{i\tilde{\vec{q}}\cdot(\vec{\rho}_l+\tilde{\vec{\lambda}}_\epsilon^m)} \times\varphi_\alpha(\vec{r}-\vec{\rho}_l-\tilde{\vec{\lambda}}_\epsilon^m)\ . \tag{29}$$

N_2^r, the number of unit cells in the normalization area, is given by $N_2/\alpha_1\alpha_2$. Vectors and functions with a tilde in the following correspond to the reconstructed surface symmetry. The expression (29) is formally equivalent to (14). Note, however, that the surface-parallel component in $\tilde{\vec{\lambda}}_\epsilon^m$ is given by $\tilde{\vec{\sigma}}_\epsilon^m$ which determines the position of atom ϵ in the mth layer of the reconstructed crystal. At the reconstructed surface there are $\alpha_1\alpha_2$ times as many atoms in the unit cell as there were in the ideal unit cell. Correspondingly the number of $\tilde{\vec{q}}$ values in the reconstructed SBZ is $1/\alpha_1\alpha_2$-times the number of $\vec{q}$ values in the corresponding ideal SBZ.

Representing the *bulk* Green's function in the new layer-orbital basis (29), we find (see the Appendix)

$$\langle m,\alpha,\epsilon;\tilde{\vec{q}}\,|\,G_b(E)\,|\,m',\alpha',\epsilon';\tilde{\vec{q}}\,\rangle = \frac{N_2^r}{N_3}\sum_i{}'\frac{L_\perp}{2\pi}\int_{-x_1}^{x_1}dk_\perp e^{i(\vec{\sigma}_\epsilon^m-\vec{\sigma}_{\epsilon'}^{m'})\cdot\vec{g}_r^i}e^{i(\vec{\kappa}^m-\vec{\kappa}^{m'})\cdot\vec{k}_\perp}\sum_n\frac{C_{\alpha m\epsilon}^n(\tilde{\vec{q}}+\vec{g}_r^i,\vec{k}_\perp)C_{\alpha' m'\epsilon'}^{n*}(\tilde{\vec{q}}+\vec{g}_r^i,\vec{k}_\perp)}{E^+-E_n(\tilde{\vec{q}}+\vec{g}_r^i,\vec{k}_\perp)}\ . \tag{30}$$

The $k_\perp$ integration extends over the same interval as in (19). The sum over i includes only a finite set of reciprocal-lattice vectors of the reconstructed surface given by (for a rectangular surface net)

$$\vec{g}_r^i=m\frac{2\pi}{b_1}\frac{\vec{b}_1}{b_1}+n\frac{2\pi}{b_2}\frac{\vec{b}_2}{b_2}\ , \tag{31}$$

with $m=0,1,\ldots,\alpha_1-1$ and $n=0,1,\ldots,\alpha_2-1$. This sum contains $\alpha_1\alpha_2$ $\vec{g}_r^i$-vectors. The $\tilde{\vec{q}}+\vec{g}_r^i$ vectors are equivalent with respect to the reconstructed surface symmetry but they are inequivalent with respect to the ideal surface symmetry. We can relate the bulk Green's function in the new representation (29) to the bulk Green's function in the ideal-surface layer-orbital representation yielding

$$\langle m,\alpha,\epsilon;\tilde{\vec{q}}\,|\,G_b(E)\,|\,m',\alpha',\epsilon';\tilde{\vec{q}}\,\rangle = \frac{N_2^r}{N_2}\sum_i{}'e^{i\vec{g}_r^i\cdot(\vec{\sigma}_\epsilon^m-\vec{\sigma}_{\epsilon'}^{m'})}\langle m,\alpha,\mu;\tilde{\vec{q}}+\vec{g}_r^i\,|\,G_b(E)\,|\,m',\alpha',\mu';\tilde{\vec{q}}+\vec{g}_r^i\,\rangle\ , \tag{32}$$

where μ and μ' have to be chosen such that $\vec{\sigma}_{\mu}^{m}$ and $\vec{\sigma}_{\epsilon}^{m}$ as well as $\vec{\sigma}_{\mu'}^{m'}$ and $\vec{\sigma}_{\epsilon'}^{m'}$ correspond to the same atom, respectively. This result transparently expresses that the ideal-surface features at the various $\tilde{\vec{q}}+\vec{g}_r^{\,i}$ points contained in the sum are "backfolded" onto $\tilde{\vec{q}}$ in the reconstructed SBZ. Off-diagonal matrix elements carry a phase factor [see (32)] which contains information about the new surface symmetry. The diagonal matrix elements, which are needed for calculating the bulk layer density of states

$$\tilde{N}^{b}_{m\alpha\epsilon}(\tilde{\vec{q}},E)=-\frac{1}{\pi}\mathrm{Im}\langle m,\alpha,\epsilon;\tilde{\vec{q}}\,|\,G_b(E)\,|\,m,\alpha,\epsilon;\tilde{\vec{q}}\rangle, \tag{33}$$

are simply given by

$$\langle m,\alpha,\epsilon;\tilde{\vec{q}}\,|\,G_{(b)}(E)\,|\,m,\alpha,\epsilon;\tilde{\vec{q}}\rangle=\frac{N_2^r}{N_2}\sum_i{}'\langle m,\alpha,\mu;\tilde{\vec{q}}+\vec{g}_r^{\,i}\,|\,G_b(E)\,|\,m,\alpha,\mu;\tilde{\vec{q}}+\vec{g}_r^{\,i}\rangle\ . \tag{34}$$

We thus find

$$\tilde{N}^{b}_{L}(\tilde{\vec{q}},E)=\frac{1}{\alpha_1\alpha_2}\sum_i{}'N_l^b(\tilde{\vec{q}}+\vec{g}_r^{\,i},E)\ , \tag{35}$$

where L is the collective index (m,α,ϵ). The bulk layer density of states at a $\tilde{\vec{q}}$ vector in the reconstructed SBZ is thus given by simple superposition of the LDOS's at the different $\tilde{\vec{q}}+\vec{g}_r^{\,i}$ points in the ideal SBZ.

Not only the bulk features become backfolded but also the electronic states of the ideal surface. This can easily be shown in our formalism. The existence condition for bound states [Eq. (8)] can be rewritten in the $|\,m,\alpha,\epsilon;\tilde{\vec{q}}\,\rangle$ representation and can again be related to the corresponding determinants in the $|\,m,\alpha,\mu;\vec{q}\,\rangle$ representation, as shown in the Appendix. The existence condition then reads

$$\tilde{D}(\tilde{\vec{q}},E)=\prod_i D(\tilde{\vec{q}}+\vec{g}_r^{\,i},E)=0\ . \tag{36}$$

This equation immediately reveals that the bound surface states which occur at any of the $\tilde{\vec{q}}+\vec{g}_r^{\,i}$ wave vectors of the ideal SBZ are found simultaneously at $\tilde{\vec{q}}$ of the reconstructed SBZ. They are thus all backfolded onto $\tilde{\vec{q}}$.

Correspondingly, the total change in the density of states introduced by an ideal surface is given at a particular $\tilde{\vec{q}}$ value of the reconstructed surface by

$$\Delta\tilde{N}(\tilde{\vec{q}},E)=\frac{1}{\alpha_1\alpha_2}\sum_i{}'\Delta N(\tilde{\vec{q}}+\vec{g}_r^{\,i},E), \tag{37}$$

showing that the changes at different $\tilde{\vec{q}}+\vec{g}_r^{\,i}$ are simply superimposed. This follows from the factorization of $\tilde{D}(\tilde{\vec{q}},E)$ which in turn leads to the result that the phase shift $\tilde{\phi}(\tilde{\vec{q}},E)$ is just the sum of the different phase shifts $\phi(\tilde{\vec{q}}+\vec{g}_r^{\,i},E)$.

Finally, the layer density of states of an ideal surface at a $\tilde{\vec{q}}$ value in the reconstructed SBZ is given by

$$\tilde{N}^{s}_{l}(\tilde{\vec{q}},E)=\frac{1}{\alpha_1\alpha_2}\sum_i{}'N_l^s(\tilde{\vec{q}}+\vec{g}_r^{\,i},E)\ , \tag{38}$$

which again demonstrates the backfolding of the ideal-surface properties onto the reconstructed surface Brillouin zone.

Until now, we have discussed the backfolding effects introduced into the ideal surface properties by layer-orbital bases appropriate for the reconstructed surface. The remaining task is to identify and to analyze the effects which occur if we switch on the reconstruction-induced interactions contained in $\mathscr{V}^{\mathrm{rec}}$. They give rise to mutual interactions between the backfolded states so that shifts and splittings can occur. These effects cannot be made transparent by analytical results. Explicit calculations are necessary and will be presented in Sec. IV. As far as the explicit form of the reconstruction matrix is concerned, we use the same prescription as discussed for the relaxed surface in connection with $\mathscr{V}^{\mathrm{rel}}$. A surface-structural model is assumed, the new interactions are calculated according to (24)—(26), and with U_s^{rec} according to (28) the surface Green's function for the reconstructed surface is calculated from Eq. (6). Also in the case of a reconstructed surface we operate with $\mathscr{V}^{\mathrm{rec}}$ only on one of the two surfaces created by U_s^{id} so that again the ideal-surface properties are obtained simultaneously for reference's sake.

One major advantage of the current method for relaxed and reconstructed surfaces, as compared to other formalisms for surface electronic structure calculations, is noteworthy, in particular. For the study of different surface-structural models the time-consuming part of the calculations, i.e., the setup of $G_b(E)$ in the appropriate layer-orbital basis, needs to be done only once in STM. Many different structures, formally described by $\mathscr{V}^{\mathrm{rel}}$ or $\mathscr{V}^{\mathrm{rec}}$ in Eqs. (23) or (28), respectively, can be dealt with by fast multiplications and inversions of small matrices. For example, in the slab approach, on the

other hand, any change of the surface geometry calls for an entirely new calculation.

III. IDEAL AND RELAXED GaAs(110) SURFACE

As a typical example for the application of the STM to relaxed surfaces we have chosen GaAs(110) which is the prototype nonpolar natural cleavage face of III-V semiconductors. This important surface has been investigated previously by several groups. We would like to mention only the more recent studies. Calandra and co-workers[4] studied GaAs(110) using the slab method based on an empirical tight-binding bulk description. Mele and Joannopoulos[5] determined electronic surface states using the transfer-matrix technique. Chadi investigated the sensitivity of the GaAs(110) surface electronic structure on surface geometry for various structural models.[6] His calculations were based, as well, on a slab geometry and an empirical tight-binding Hamiltonian, which retains only first-nearest-neighbor interactions. Tougaard[7] has studied the electronic properties of (110) surfaces of zinc-blende crystals using the Green's-function method. His calculations could be performed analytically since they were based on a simplified tight-binding model. More realistic investigations of various (110) surfaces of zinc-blende crystals have been carried out by Dow and co-workers[20] who used first-nearest-neighbor sp^3s^* Hamiltonians. Self-consistent studies of GaAs(110) have been reported as well. Chelikowski and Cohen[8] used local pseudopotentials in their study while Zunger[9] recently reported the results of self-consistent surface electronic structure calculations based on nonlocal pseudopotentials.

Numerous experimental investigations have shown that the GaAs(110) surface relaxes after cleavage without changing the size or the symmetry of the surface unit cell. The unit cell contains one anion and one cation, as shown in Fig. 1. Each surface-layer cation (labeled C_1 in figure) is bonded to two surface-layer anions (A_1 and A_1') and to one anion (A_2) on the first subsurface layer. The fourth cation bond is broken and left dangling upon surface creation. The surface-layer anions have the corresponding cation-neighbor configuration and one of the As bonds is broken and left dangling on the surface as well. At present, the generally accepted surface-structural model is the bond-angle relaxation model.[21] In this model the surface-layer As atoms move outward and the surface-layer Ga atoms move inward in the y-z plane (see Fig. 1 for coordinate system) without destroying the mirror symmetry of the (110) surface. The atomic movements lead to a tilt angle of the surface Ga—As bond of about 27° with respect to the ideal surface plane. This geometry results from an analysis of inelastic low-energy electron diffractions (ILEED) data[21,22] and is in accordance with the results of total-energy minimization calculations.[23] We have based our cal-

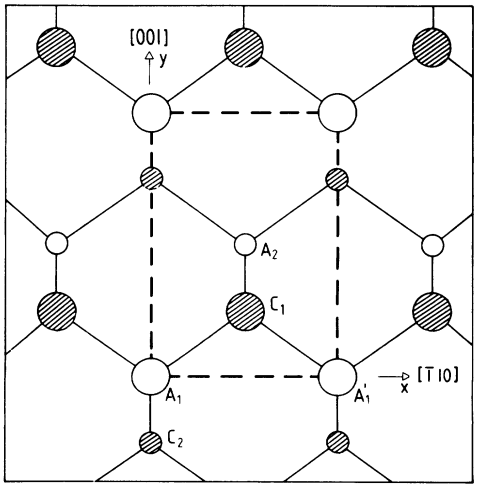

FIG. 1. Arrangement of atoms in the topmost layers of ideal GaAs(110). Shaded circles denote cations and open circles denote anions.

TABLE I. Empirical tight-binding parameter sets for GaAs and Si. The Si parameters are from Ref. 46. Energies are in eV, the zero of the energy scale is the top of the valence bands.

Parameter	GaAs	Si
E_s^c	−3.0	−4.2
E_p^c	1.40	0.19
E_s^a	−7.51	−4.2
E_p^a	0.28	0.19
V_{ss}^1	−1.76	−2.08
V_{sp}^{ca}	1.98	2.12
V_{sp}^{ac}	2.46	2.12
$V_{pp\sigma}^1$	2.49	2.32
$V_{pp\pi}^1$	−0.32	−0.52
V_{ss}^{cc2}	−0.05	
V_{ss}^{aa2}	−0.03	
$V_{pp\sigma}^{cc2}$	0.65	0.58
$V_{pp\sigma}^{aa2}$	0.40	0.58
$V_{pp\pi}^{cc2}$	−0.16	−0.1
$V_{pp\pi}^{aa2}$	0.05	−0.1

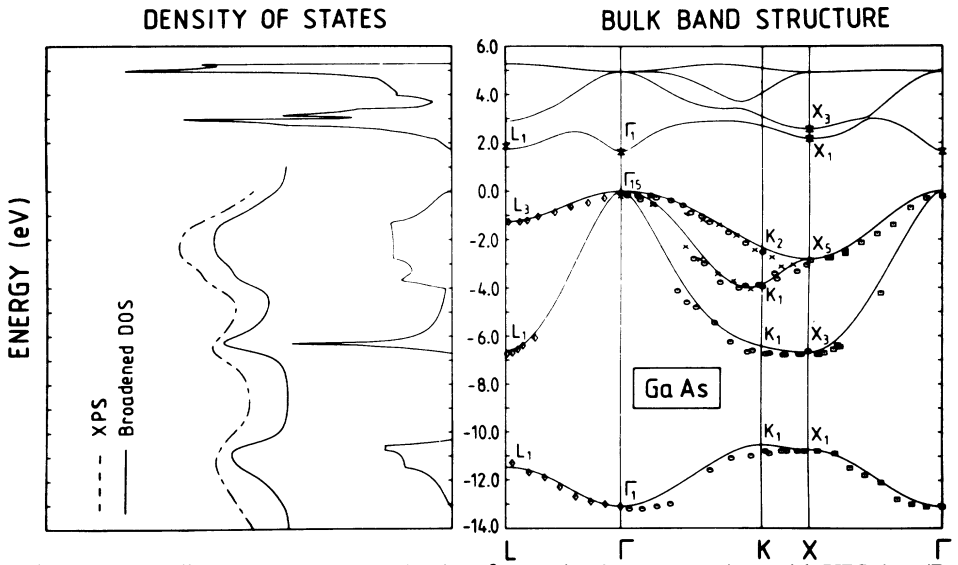

FIG. 2. Calculated GaAs bulk band structure and density of states in direct comparison with UPS data (Ref. 24), reflectivity data (Ref. 25), and XPS data (Ref. 26). Our valence-band DOS is also shown after Lorentzian broadening (by 0.25 eV) in order to ease the comparison with the XPS spectrum of Ref. 26.

culations on the structural model worked out by Chadi.[13,14] The anions and cations are displaced by

$$\Delta y_a = 0.18, \quad \Delta z_a = 0.19,$$

$$\Delta y_c = 0.35, \quad \Delta z_c = -0.46,$$

in angstrom (Å) units, where z is perpendicular to the surface plane and y lies in the surface plane (see Fig. 1).

Having specified the surface system, we can now apply the formalism of Sec. II. First, we have to set up an empirical tight-binding description of bulk GaAs. We have determined the parameters defining our bulk Hamiltonian by fitting experimental UPS data[24] and reflectivity data.[25] The parameters are given in Table I. Figure 2 shows our GaAs bulk band structure and density of states (DOS) together with the experimental UPS, reflectivity, and x-ray photoemission spectroscopy (XPS) data.[26] It should be noted that we have used in the fitting procedure only the UPS and reflectivity data at Γ, X, and L. Figure 2 convincingly demonstrates that the resulting ETBM bulk Hamiltonian nicely reproduces the measured band structure throughout the bulk Brillouin zone. This good agreement for the occupied states is further confirmed by the favorable comparison between the calculated DOS and the XPS spectrum of Ley *et al.*[26] Even the lowest conduction band is in excellent agreement with the reflectivity data of Aspnes *et al.*[25] This good agreement is reached, however, on the expense of less-accurate higher conduction bands. In particular, the total conduction-band width in our bulk band structure is too small, a problem which is inherent in second-nearest-neighbor ETBM bulk descriptions. This shortcoming could be removed by either taking into account third-nearest-neighbor interactions[27] or taking into account d orbitals. Both cures considerably enhance the complexity of the calculations without yielding any relevant changes within the valence bands.[28] Since we are mainly interested in the ground-state properties of the surface system, i.e., in the *occupied* states and resonances within the projected valence bands, our Hamiltonian is optimally suited for the calculations. It goes without saying that care is needed in the interpretation of the results for empty surface states.

In Figs. 3(a) and 3(b) we show the surface band structures for the ideal and the relaxed GaAs(110) surface in direct comparison. The projected bulk band structure is plotted as a point pattern which gives a visual impression of the density of projected bulk states at any given $\vec{k}_{\parallel}$ and E. The origin and nature of the various surface-state bands can most easily be analyzed by considering the corresponding wave-vector–resolved layer densities of states. Typical examples for the ideal and the relaxed surface are given in Figs. 4(a) and 4(b).

Let us first briefly summarize the properties of the ideal surface shown in Figs. 3(a) and 4(a). There are four pronounced bands of surface states S_a, S_c, D_a, and D_c. They are anion or cation derived, as indicated by the indices, and are either mainly s-like backbond states or predominantly p-like dangling-bond states, respectively. Figure 4(a) reveals the

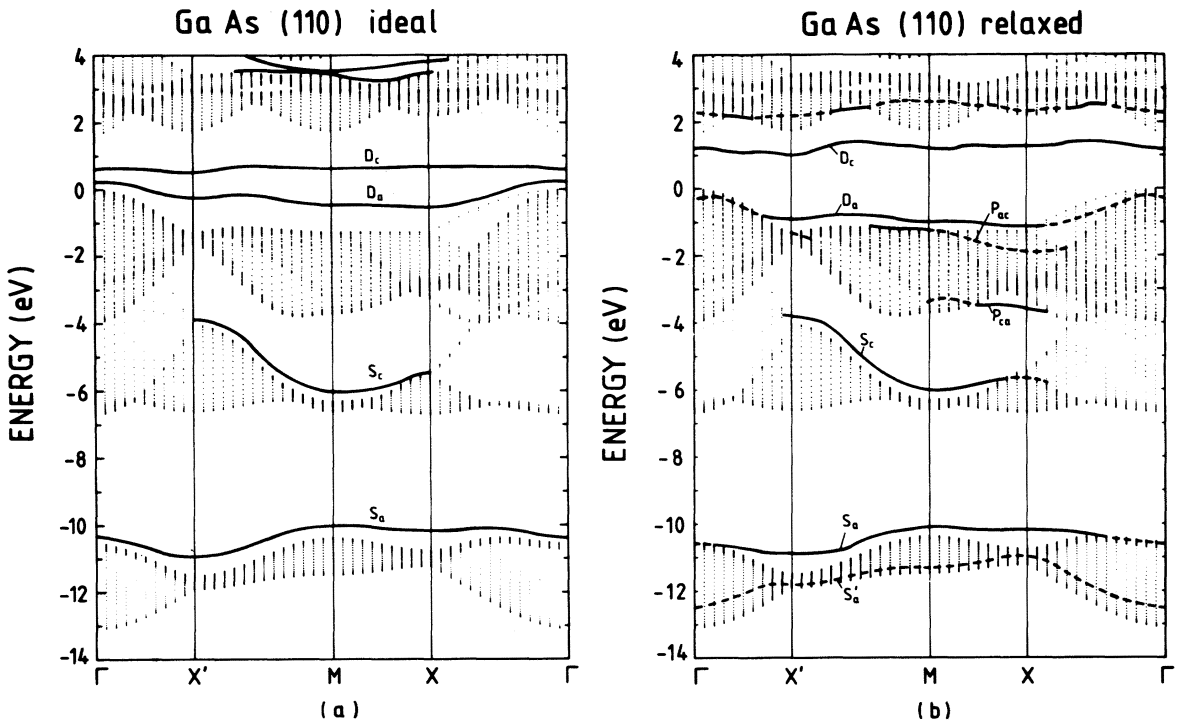

FIG. 3. Surface electronic structure for ideal (a) and relaxed (b) GaAs(110) surface. The labeling of various surface features is discussed in detail in the text.

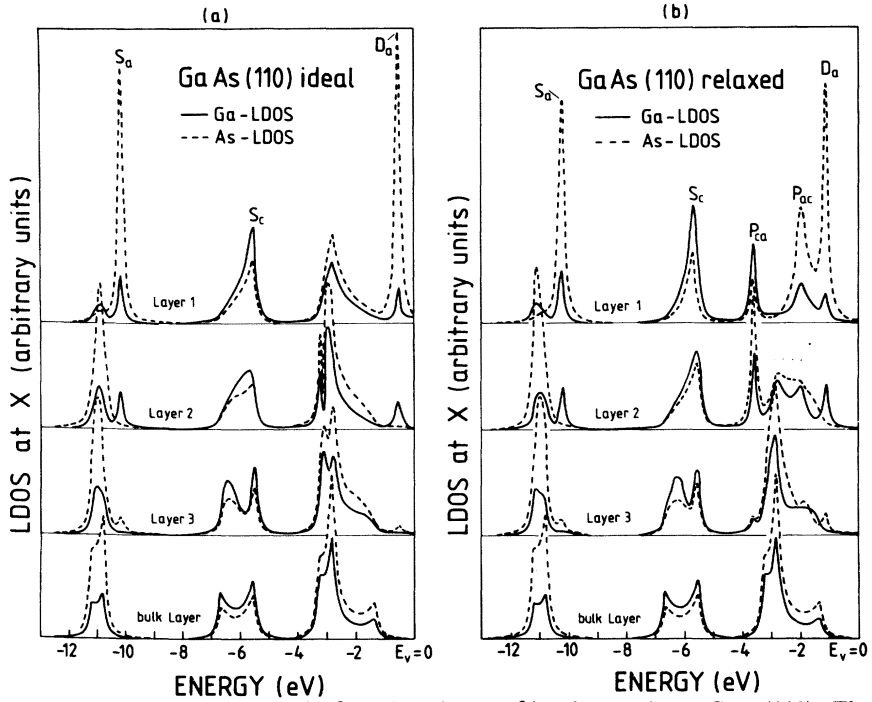

FIG. 4. Wave-vector—resolved LDOS's on the first three layers of ideal and relaxed GaAs(110). The bulk layer DOS is given for further comparison.

atomic character of the different surface states at the X point. Our cation-derived dangling-bond band D_c [see Fig. 3(a)] lies too low in energy by about 0.5 eV, as compared to the results of other calculations. This is an artifact resulting from the too small conduction-band width of our bulk Hamiltonian.

The changes in the surface electronic structure, induced by the bond-angle relaxation are shown in Figs. 3(b) and 4(b). Since these results are relevant for the interpretation of experimental data on occupied surface states, we have included in Fig. 3(b) pronounced resonances by dashed lines as well. We see that the surface relaxation has only very small influence on the bands S_a and S_c. The reason for this result lies in the fact that nearest-neighbor distances are changed in the present relaxation model at most by 3%, so that s states are only marginally affected. The mainly p-like-bonding band region between -4 and 0 eV is strongly influenced by the bond-direction and bond-length changes at the relaxed surface. Note the dramatic change in the surface-layer and subsurface-layer densities of states between the ideal and the relaxed surface in this energy range (see Fig. 4). The figure demonstrates that the electronic structure very sensitively reacts to surface-geometrical changes. First, we note that the occupied dangling-bond band D_a moves down in energy (almost rigidly) by about 0.8 eV upon relaxation, thus lowering the total energy of the system. In addition new relaxation-induced states (resonances) P_{ca} and P_{ac} occur, which are p-like in nature. They result from the second-nearest-neighbor distance and bond-direction changes between surface-layer cations (anions) and subsurface-layer anions (cations), as compared to the ideal surface binding environment. These changes give rise to a rehybridization of the sp^3 orbitals at the atoms in the surface region. The inward rotation of the cation is responsible for the creation of the state P_{ca} whereas the outward rotation of the anion causes the state P_{ac}.

The high sensitivity of surface states and resonances with respect to relaxation shows that comparing the results of surface electronic structure calculations with ARUPS data can indeed be a helpful tool in confirming surface-structural models proposed on the basis of LEED analyses. We have reported in a short communication[16] calculations of angle-resolved initial-state spectra (ARISS) using the scattering-theoretical method on the basis of our bulk Hamiltonian for the present relaxation model. Comparing the calculated ARISS's with measured angle-resolved electron-density curves (AREDC's) we arrived at a detailed interpretation of the experimental data (see Ref. 16). To emphasize this point, we present in Table II a comparison of calculated and measured peak positions[29–32] at X. The table convincingly demonstrates that both bulk-derived as well as surface-derived peaks in the calculated angle-resolved initial-state spectra at the X point nicely agree with the experimental data. This agreement proves that we have arrived at a quantitative description of the occupied surface states.

TABLE II. Measured peak positions in ARUPS spectra for GaAs(110) in comparison with theoretical results. The experimental detector geometry corresponds to the X point in the surface Brillouin zone. The theoretical results are peak positions in the bulk layer DOS, on the one hand, and peak position in the angle-resolved initial-state spectra. Energies are measured in eV relative to the top of the valence band, at $E_V=0$ eV.

Theory		Experiment			
Bulk	ARISS	Ref. 29	Ref. 30	Ref. 31	Ref. 32
−5.5	−5.7	−5.55			
	−3.6	−3.6			−4.0
−2.8	−2.8	−3.0	−2.8	−2.9	−2.7
	−2.0	−2.1	−1.8	−2.1	−2.2
	−1.2	−1.2		−1.2	−1.0

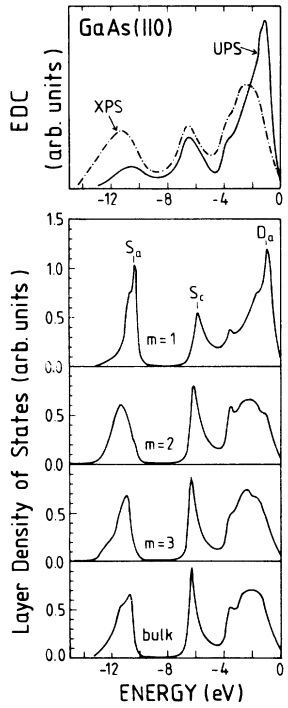

FIG. 5. Comparison of XPS (Ref. 26) and UPS (Ref. 34) spectra with calculated LDOS's (angle-integrated) on the first three layers of GaAs(110) and on a bulk layer. Pronounced surface features are labeled according to their nature [see also Figs. 3(b) and 4(b)].

The empty dangling-bond band D_c is shifted up in energy by about 0.6 eV (again almost rigidly) upon relaxation (see Fig. 3). Nevertheless, it still resides within the projected band gap. The *relative* relaxation-induced *shift* is in good agreement with the result of other calculations. The *absolute position* of our band D_c is not in good agreement with other theoretical or with experimental results[33] for the reasons discussed already in connection with the bulk conduction bands and with the band D_c at the ideal surface.

We conclude our discussion of the application of the STM to the relaxed GaAs(110) surface with a comparison of wave-vector–integrated layer densities of states on the first, second, and third surface layer as well as on a bulk (110) layer with measured XPS and UPS spectra.[26,34] This comparison is made in Fig. 5. The figure explains that the main changes in the UPS spectrum, as compared to the XPS spectrum, are induced by the anion backbond band S_a, the cation-dominated backbond S_c, and most pronounced by the As dangling-bond band D_a. We find very good agreement between the peak positions in the calculated LDOS's and the measured EDC's.

IV. IDEAL AND 2×1 RECONSTRUCTED Si(100) SURFACE

For our first application of the STM to a reconstructed surface, we have chosen Si(100)-(2×1). LEED (Ref. 35) and He-diffraction[36] data show that Si(100) undergoes either a 2×1, 2×2, or 4×2 reconstruction. The 2×1 pattern seems to be by far the most dominant. In the present paper we discuss only the electronic structure of the 2×1 reconstructed surface. Various structure models have been proposed for this surface. We mention the vacancy model,[37] the conjugated-chain model,[38] the pairing model,[39] and the asymmetric dimer model.[13,14,40] The first three of these models had to be discarded[41,42] since they yield electronic densities of states[11,12] which disagree with photoemission data.[41] Only the asymmetric dimer model[13,14,40] yields a semiconducting surface, in agreement with experiment.[41] Further support for this model was obtained by dynamical LEED analyses,[35] by ion-beam crystallography,[43] and by core-level spectroscopy data.[44] Very recently, a generalized valence-bond orbital calculation based on a molecular geometry by Redondo *et al.*[45] has been published, which yields a *symmetrical* surface dimer as the building block of the reconstruction. This finding contradicts earlier total-energy–minimization calculation results[13,14,40] and the experimental evidences for the asymmetric dimer geometry.[35,43,44] In our calculations we have used, therefore, the surface-structure model of Ihm, Cohen, and Chadi.[14] Using that model, we can directly compare our theoretical results with the results of Refs. 13 and 14.

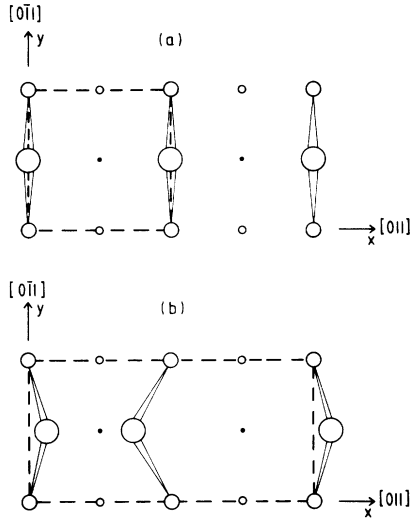

FIG. 6. Surface geometry of the (a) ideal Si(100) surface and (b) the 2×1 reconstructed Si(100) surface. The corresponding unit cells are shown by heavy dashed lines. The largest circles show surface-layer atoms. The atoms on the following three layers are shown as well.

The arrangement of atoms at the ideal and at the 2×1 reconstructed surface is shown in Fig. 6. In the asymmetric dimer model, Si surface-layer atoms become displaced in a way that is similar to the Ga and As atom movements at the relaxed GaAs(110) surface. The two Si atoms considered move towards each other so that they essentially become first-nearest neighbors. In addition one of the two atoms moves outwards (in the following referred to as the "up" atom) whereas the second atom moves inward (referred to as the "down" atom). This is similar to the bond-angle relaxation at GaAs(110). The Si–surface-atom displacements are[14]

$$\Delta x_{\text{up}}=0.46, \qquad \Delta z_{\text{up}}=0.04\ ,$$
$$\Delta x_{\text{down}}=-1.08, \quad \Delta z_{\text{down}}=-0.435\ ,$$

in units of Å, where z is perpendicular to the surface plane and x lies in the surface plane [see Fig. 6(b)].

We have evaluated the surface electronic structure of the semi-infinite Si crystal terminated by the ideal (100) surface and by the reconstructed 2×1 surface. The bulk crystal is described by the ETBM Hamiltonian of Pandey and Phillips[46] which retains first-nearest-neighbor and some second-nearest-neighbor

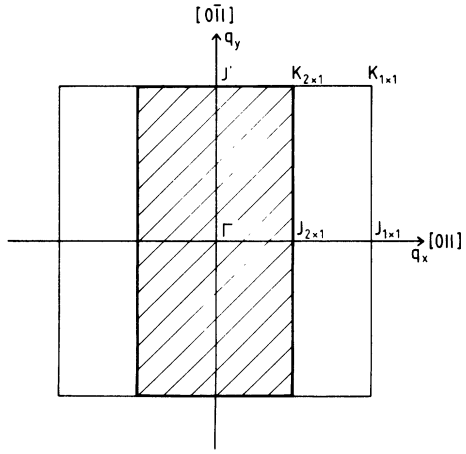

FIG. 7. Surface Brillouin zones of the ideal 1×1 and the reconstructed 2×1 surfaces of Si(100). High-symmetry points have been labeled according to the surface geometry [ideal (1×1) and reconstructed (2×1)]. Note that the Γ and J' points are not changed by a 2×1 reconstruction.

interaction matrix elements. The parameters are listed in Table I.

We begin our discussion of Si(100) with the ideal surface. The surface Brillouin zones for the 1×1 and the 2×1 surfaces are shown in Fig. 7. We will present the ideal surface-band structure using the 2×1 unit cell. This means that we have to fold back the ideal surface-band structure, which was given already in Ref. 1, onto the 2×1 zone. The backfolding process superimposes the projected bulk states and the surface states of the 1×1 zone onto the 2×1 zone. The result is shown in Fig. 8. First we note that the surface states in that figure between $J_{2\times1}$ and $K_{2\times1}$ are all twofold degenerate (apart from spin degeneracy) since the $J_{2\times1}K_{2\times1}$ line is folded onto itself (see Fig. 7). The full lines in Fig. 8 are all surface-state bands which belong to bound states at the ideal surface. Those which coincide with the projected bulk bands of the 2×1 surface Brillouin zone become resonant with bulk states due to the reconstruction-induced surface umklapp. We have discussed this effect in detail in Sec. II. The prominent features of the ideal surface electronic structure are the predominantly s-like backbond bands around -6 and -9 eV, which correspond to the bands S_c and S_a at the GaAs(110) surface and the dangling-bond and bridge-bond band D and Br, respectively, which occur in the band-gap energy region. Note that large parts of the backfolded dangling-bond band are resonant with bulk states. They can couple to the latter at the reconstructed surface due to the reduced symmetry which yields new selection rules.

The surface-band structure for the reconstructed surface is shown in Fig. 9. We have plotted true bound states as full lines and indicated surface resonances (which were not shown in Fig. 8 for the ideal surface) by dashed lines. In the energy region below -6 eV we find five bands of surface states (resonances) which all have strong s character. The states S_1 and S_2 are entirely reconstruction induced while S_3—S_5 correspond to the backbond states B_1—B_3, already present at the ideal surface. Of course, S_3—S_5 are slightly shifted in energy, as compared to B_1—B_3. Between -5 and 0 eV we find five bands of surface states which are predominantly p-like (P_1—P_5). One of these bands, namely P_3, can be identified as the dimer-bond band. Within the band-gap energy region four bands of surface states (labeled $D_{\rm up}$, $D_{\rm down}$, P'_1, and P'_2) are found.

The origin, the character, and the localization properties of the various surface states (resonances) can again be inferred from atom-, orbital-, and wave-vector—resolved layer densities of states. In Fig. 10, we show one example, namely the LDOS's on the first three layers at the K point in direct comparison with the corresponding bulk layer density of states. The figure clearly shows the character and strength of the various surface features at the K point (see Fig. 9 for comparison). It highlights their localization properties and indicates how the surface features are related to underlying bulk electronic properties. Within the STM it is easy to identify the orbital character of the various surface features in great detail. This is exemplified in Fig. 11, where we analyze the surface layer DOS at the K point in the energy region from -5 to $+3$ eV (see Fig. 10 for comparison) with respect to the up and down atoms in the surface unit cell and with respect to their p_z,s,p_x,p_y wave-function character. Remember that z is perpendicular to the surface and that x is the dimer-bond direction. Figures 10 and 11 convincingly demonstrate that $D_{\rm up}$ is a dangling-bond state at the up atom, while $D_{\rm down}$ is a dangling-bond state at the down atom. Both features have very strong p_z contributions. The p_x contribution gives rise to a tilt angle of these two dangling bonds with respect to the (100) plane (see the inset for comparison). The dangling bond at the up atom has considerable s admixture which lowers its energy position relative to $D_{\rm down}$. The band $D_{\rm up}$ is fully occupied, whereas $D_{\rm down}$ is empty, the two bands being separated by an indirect gap of 0.15 eV. Therefore, the surface is semiconducting, in agreement with experiment. The states P'_1 and P'_2 lie both close to the conduction-band edge. Having a dominant p character, they can be considered as the

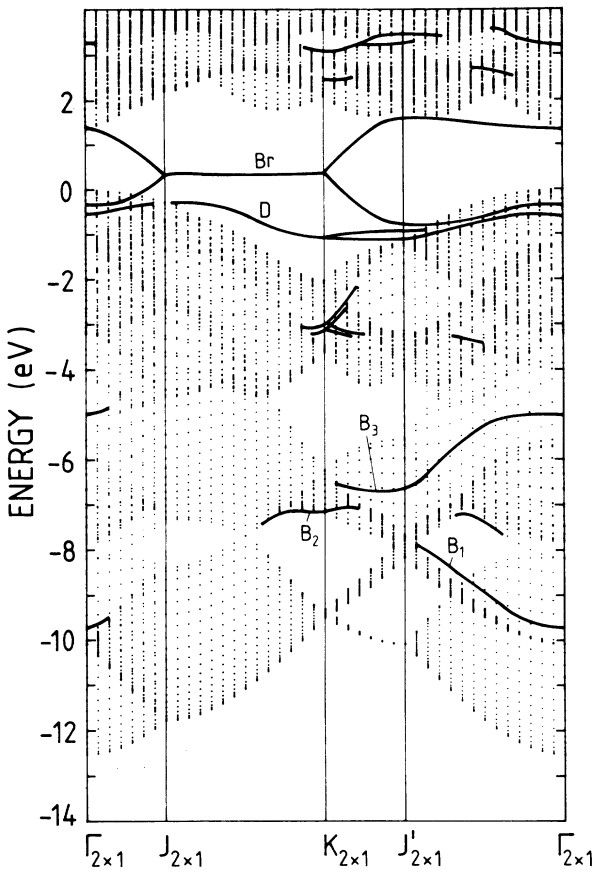

FIG. 8. Surface-band structure of ideal Si(100) backfolded onto the 2×1 surface Brillouin zone. The bridge-bond band, the dangling-bond band, and the backbond bands are labeled Br, D, and B_1 to B_3, respectively.

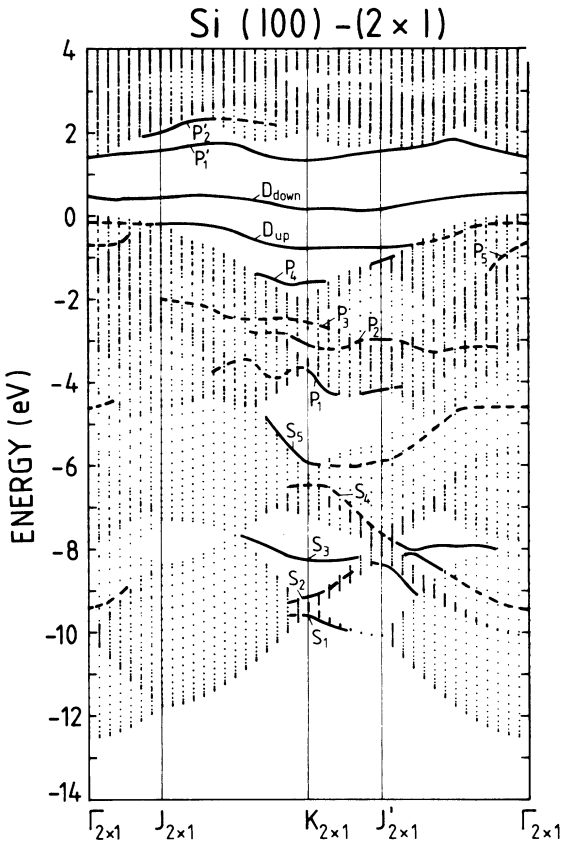

FIG. 9. Surface-band structure of Si(100)-(2×1) for the asymmetric dimer model. The surface-state bands are labeled according to their origin and nature. For details see the discussions in the text.

antibonding states of P_3–P_5.

These results lead us to conclude that the major effects of reconstruction occur in the band-gap energy region, as a consequence of the rehybridization of the p orbitals following the displacement of the two surface atoms. Indeed, as compared to the ideal surface, the dimerization leads to an enhanced interaction between the p_z orbitals and the p_x orbitals on the two atoms. Henceforth, the degeneracies of the dangling-bond (D) and the bridge-bond (Br) bands in the backfolded band structure of the ideal surface (see Fig. 8) are lifted between $J_{2\times1}$ and $K_{2\times1}$ and the resulting states repel each other. Owing to the fact that the p_x orbitals interact through a $V_{pp\sigma}$ interaction, and the p_z orbitals interact through a much weaker $V_{pp\pi}$ interaction, the shift of the bridge-bond states is much stronger than the shift of the dangling-bond states. As a consequence, the bridge-bond states enter into the projected bulk band regions and interact with these bulk bands. In the valence-band region they disappear, except for $\tilde{\bar{q}}$ values between $J_{2\times1}$ and $K_{2\times1}$ where the dimer-bond state P_3 subsists. For the asymmetric dimer these shifts are stronger than for the symmetric dimer, as the asymmetric dimer allows p_x (p_z) orbitals on the up atom to interact with p_z (p_x) orbitals on the down atom, giving rise to a charge transfer from the down atom to the up atom. This behavior is similar to that of the relaxed GaAs(110) surface, the up atom playing the role of the anion and the down atom playing the role of the cation.

We turn now to a brief comparison of some of our results with the available experimental data. Angle-resolved photoemission measurements have been reported by Himpsel and Eastman,[41] van Hoof and van der Wiel,[47] and Uhrberg *et al.*[48] All experiments seem to show that the surface is semiconducting, which is in agreement with our theoretical results. In all experiments a structure is observed in the energy region just below the top of the valence

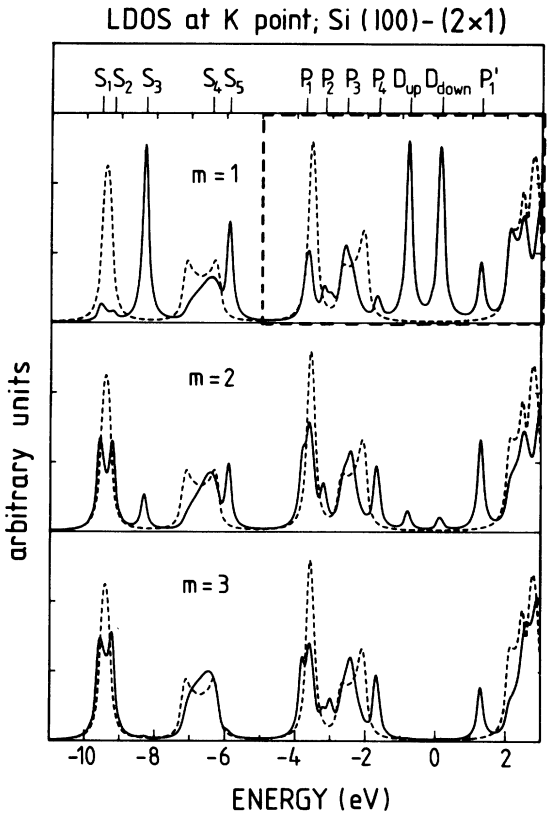

FIG. 10. Wave-vector—resolved layer densities of states on the first three layers of the reconstructed Si(100)-(2×1) surface at the K point. The bulk layer DOS is shown for comparison by dashed lines. Pronounced peak positions are labeled according to the nomenclature introduced in Fig. 9. For the dashed box in the uppermost panel, see Fig. 11.

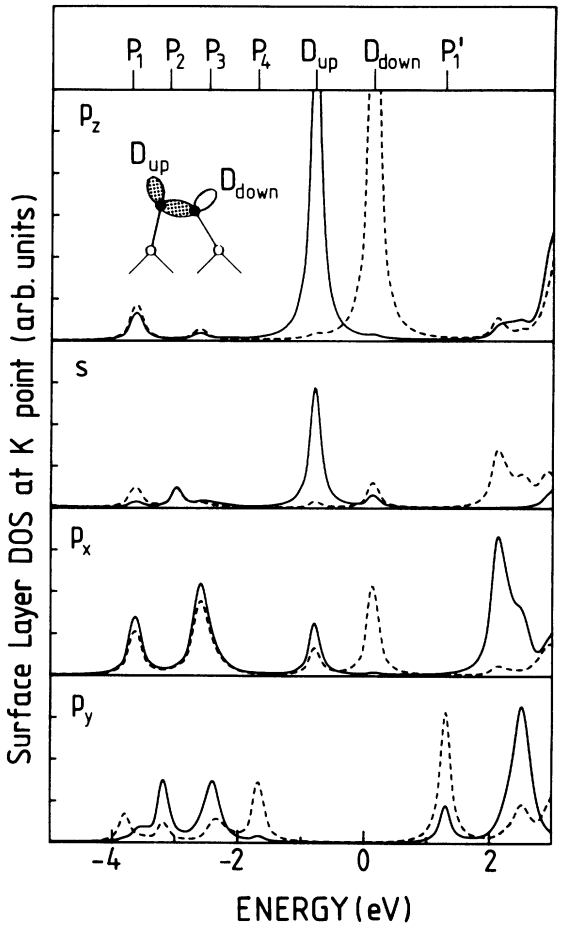

FIG. 11. Atom- and orbital-resolved density of states on the surface layer of Si (100)-(2×1) at the K point (corresponding to the dashed box in Fig. 10). The full lines show the LDOS on the "up" atom and the "down" atom contribution is shown by the dashed lines. The dangling orbitals corresponding to D_{up} and D_{down} are shown schematically in the inset.

bands which corresponds to the occupied, lower dangling-bond state D_{up}. In Fig. 12 we compare our calculated dispersion of the D_{up} band with the experimental data of Refs. 41, 47, and 48. Note that our calculated surface-state band is in very good agreement with the experimental data as far as the energetic position, the dispersion, and the bandwidth are concerned. The theoretical bandwidth is 0.6 eV whereas experimentally one observes 0.5,[41] 0.7,[47] and 0.65 eV.[48]

We have included, as well, in Fig. 12 the D_{up} band as it results from Refs. 13 and 14, respectively.[49] In Ref. 13 this band is a factor of 2 too wide which results from the used first-nearest-neighbor bulk Hamiltonian. The self-consistently calculated band from Ref. 14 agrees better in dispersion with the experimental data but lies roughly 0.8 eV too high in energy.

In addition to the dangling-bond state, Uhrberg *et al.*[48] found a surface state in the energy range from −2 to −2.3 eV, which disperses downward in energy from the middle of the $J_{2\times1}K_{2\times1}$ line to the $K_{2\times1}$ point. This feature was attributed to the dimer bond and it corresponds very well with our dimer-bond band P_3 extending from $J_{2\times1}$ to $K_{2\times1}$.

Himpsel and Eastman[41] have reported a second state above the projected valence bands at $J'_{2\times1}$ which lies about 0.6 eV above D_{up}. There is no indication for such a state in our results for the 2×1 surface. This feature, as well, was not reported by the other experimental groups. In Ref. 47 it is suggested that this feature could be due to the presence

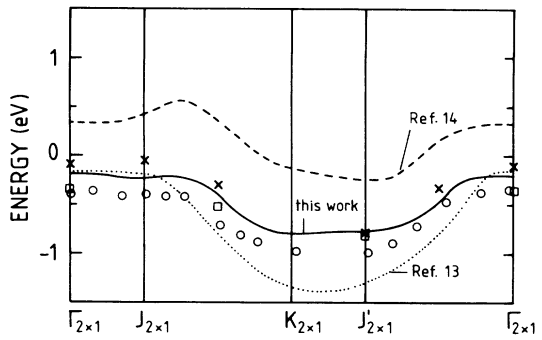

FIG. 12. Comparison of the experimentally determined dispersion of the most prominent occupied surface state at the Si(100)-(2×1) surface with our calculated band D_{up} (full line) and with the corresponding bands of Refs. 13 and 14. The experimental data points are taken from Ref. 41 (□), Ref. 47 (×), and Ref. 48 (○).

of additional domains of other reconstructions like 2×2 or 4×2. Indeed both would lead to an additional backfolding which superimposes $\Gamma_{2\times1}$ on $J'_{2\times1}$ and could henceforth explain the experimentally observed second peak. Experimental observations of other states have not been reported up to now.

V. SUMMARY

We have presented the formal extensions of the scattering-theoretical method necessary for the treatment of relaxed and reconstructed surfaces. We have illustrated the various advantages and the high effectivity of the method when it is used in conjunction with an empirical tight-binding bulk description. Backfolding of ideal surface states at a reconstructed surface were made transparent analytically. Using realistic bulk Hamiltonians which retain first- and second-nearest-neighbor interactions, we have applied the STM to the relaxed GaAs(110) surface and to the reconstructed Si(100)-(2×1) surface. The evaluation of the GaAs(110) surface electronic structure of the 27° bond-angle rotation model yields wave-vector–integrated LDOS's as well as angle-resolved initial-state spectra which were found to be in good agreement with experimental data. An analysis of the surface electronic structure for the asymmetric dimer model of Si(100)-(2×1) has shown good agreement between the available ARUPS data and our results. This holds in particular for the most prominent surface-induced feature, namely the occupied dangling-bond band originating from the up atom in the dimer.

ACKNOWLEDGMENT

Financial support by the Deutsche Forschungsgemeinschaft is gratefully acknowledged.

APPENDIX

In this appendix we set up the expression for the bulk Green's function in the layer-orbital representation $\{|m,\alpha,\epsilon;\tilde{\vec{q}}\rangle\}$; i.e., the layer-orbital representation of the reconstructed surface unit cell. We restrict our discussion to the case of a 2×1 reconstruction of a (100) surface of an fcc lattice. The general case can be treated along the same lines.

The bulk Green's function is given in the layer-orbital representation by

$$\langle m,\alpha,\epsilon;\tilde{\vec{q}}\,|\,G_b(E)\,|\,m',\alpha',\epsilon';\tilde{\vec{q}}\rangle = \sum_{n,\vec{k}} \frac{\langle m,\alpha,\epsilon;\tilde{\vec{q}}\,|\,n,\vec{k}\rangle\langle n,\vec{k}\,|\,m',\alpha',\epsilon';\tilde{\vec{q}}\rangle}{E^+ - E_n(\vec{k})}\ , \tag{A1}$$

where ϵ and ϵ' run over the two atoms in the reconstructed unit cell.

Inserting the expressions (12), (13), and (29) in Eq. (A1) yields

$$\langle m,\alpha,\epsilon;\tilde{\vec{q}}\,|\,G_b(E)\,|\,m',\alpha',\epsilon';\tilde{\vec{q}}\rangle = \frac{N_2^r}{N_3} \sum_{n,\vec{k}_\perp} \sum_i{}' \frac{e^{i(\vec{\sigma}^m_\epsilon - \vec{\sigma}^{m'}_{\epsilon'})\cdot\vec{g}^i_r} e^{i(\vec{\kappa}^m - \vec{\kappa}^{m'})\cdot\vec{k}_\perp}}{E^+ - E_n(\tilde{\vec{q}}+\vec{g}^i_r,\vec{k}_\perp)} \times C^n_{m\alpha\epsilon}(\tilde{\vec{q}}+\vec{g}^i_r,\vec{k}_\perp) C^{n*}_{m'\alpha'\epsilon'}(\tilde{\vec{q}}+\vec{g}^i_r,\vec{k}_\perp)\ . \tag{A2}$$

The sum over $\vec{g}^i_r$ runs only over a restricted set of reciprocal-lattice vectors. For a given $\tilde{\vec{q}}$ only those $\vec{g}^i_r$ must be included, for which $\vec{q}+\vec{g}^i_r \equiv \vec{k}_{||}$ lies within the projection of the first bulk Brillouin zone onto the (100) surface plane. It is very important to note that the boundaries for the summation over $\vec{k}_\perp$ in (A2) depend sensitively on $\vec{g}^i_r$. The vectors $\vec{\lambda}^m_\epsilon$ are defined analogously to $\vec{\lambda}^m_\mu$ [see relation (15)] so that the set $\{\vec{\rho}_l, \vec{\lambda}^m_\epsilon\}$ spans the entire bulk lattice.

In order to discuss the various reciprocal-lattice vectors entering the sums in (A2), we show in Fig. 13 the surface Brillouin zone (SBZ) together with

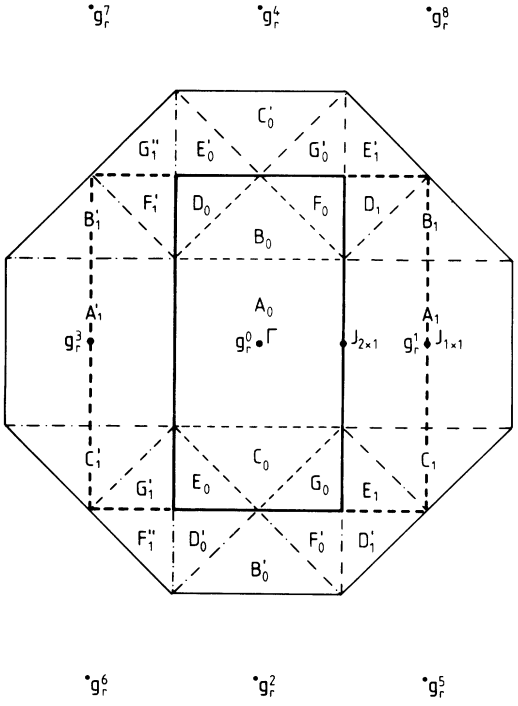

FIG. 13. Surface Brillouin zone for the ideal 1×1 and for the reconstructed 2×1 Si(100) surface (heavy line) together with the projection of the three-dimensional bulk Brillouin zone onto the (100) plane. The various $k_{||}$ regions inside the SBZ of the 2×1 surface (A_0 to G_0) and outside the SBZ but inside the projected *bulk* Brillouin zone, which need to be considered for the sums in Eq. (A2), are labeled explicitly. The heavy dots show reciprocal-lattice points reached by the $\vec{g}_r^i$ vectors of the 2×1 surface. For more details, see text.

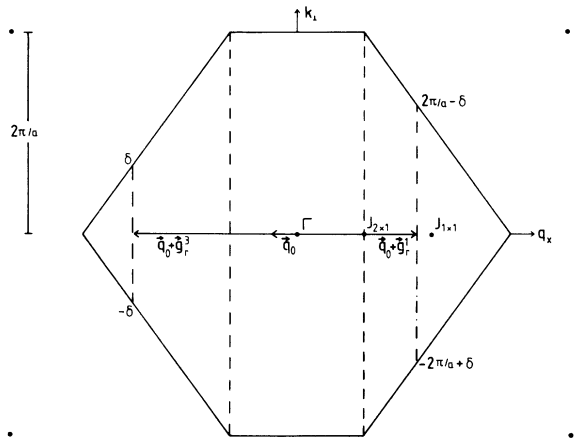

FIG. 14. Cut of the bulk Brillouin zone perpendicular to the (100) surface containing the line Γ-$J_{2\times1}$-$J_{1\times1}$. For details see the Appendix.

the projection of the bulk Brillouin zone onto a (100) plane. The SBZ has been subdivided into areas A_0 to G_0. For $\tilde{\vec{q}}$ vectors lying in one of these different areas, different boundaries on the $\vec{k}_\perp$ sum have to be implied. Consider, for example, a $\tilde{\vec{q}}$ residing in the central area A_0. In this case, the reciprocal-lattice vectors $\vec{g}_r^0$, $\vec{g}_r^1$, and $\vec{g}_r^3$ have to be retained in Eq. (A2). For $\vec{g}_r^i=\vec{g}_r^0$, the $\vec{k}_\perp$ sum in (A2) runs from the bottom to the top of the first bulk Brillouin zone, i.e., from $-2\pi/a$ to $2\pi/a$. For $\vec{g}_r^i=\vec{g}_r^1$, we find that the $\vec{k}_\perp$ integration runs only from $-2\pi/a+\delta$ to $2\pi/a-\delta$ as shown in Fig. 14. The figure shows as well, the $\vec{k}_\perp$ summation interval for $\vec{g}_r^i=\vec{g}_r^3$, which is $-\delta<\vec{k}_\perp\leq\delta$.

Using bulk symmetry, it is simple to show that the $\vec{g}_r^1$ and the $\vec{g}_r^3$ contributions with their appropriate $\vec{k}_\perp$ regions are equivalent to one single, say, $\vec{g}_r^1$ contribution with $-2\pi/a<k_\perp\leq2\pi/a$ as boundaries for the $\vec{k}_\perp$ sum. This is seen as follows: The bulk wave functions and energies obey the following symmetry requirements:

$$C_{\alpha\nu}^n(\vec{k})=C_{\alpha\nu}^n(\vec{k}+\vec{G})e^{i\vec{G}\cdot\vec{\tau}_\nu}, \tag{A3}$$

and

$$E_n(\vec{k})=E_n(\vec{k}+\vec{G}), \tag{A4}$$

where $\vec{G}$ is a reciprocal-lattice vector of the three-dimensional bulk lattice.

If we choose

$$\vec{G}=(-2\vec{g}_r^3,\mp2\pi/a), \tag{A5}$$

we can rewrite $\vec{k}=\tilde{\vec{q}}+\vec{g}_r^3+\vec{k}_\perp$, by adding a bulk reciprocal-lattice vector $\vec{G}$, as

$$\vec{k}+\vec{G}=(\tilde{\vec{q}}+\vec{g}_r^1,\vec{k}_\perp), \tag{A6}$$

where now $k_\perp$ runs from $-2\pi/a$ to $-2\pi/a+\delta$ and over $2\pi/a-\delta$ to $2\pi/a$ [see Fig. 14]. In other words, combining the contributions due to $\vec{g}_r^1$ and $\vec{g}_r^3$ is equivalent to taking only the term with $\vec{g}_r^1$ and extending the $\vec{k}_\perp$ summation over the full interval from $-2\pi/a$ to $+2\pi/a$. Thus only two reciprocal-lattice vectors need to be taken into account effectively, as one would have expected for a 2×1 surface. With the help of Figs. 13 and 14 and Table III, it is simple to go through the same symmetry considerations for $\tilde{\vec{q}}$ vectors lying in the other areas B_0 to G_0 of the SBZ. For every $\tilde{\vec{q}}$ region in the SBZ, Table III lists the $\vec{g}_r^i$ vectors contributing to the sum (A2) together with the corresponding region of the projected bulk Brillouin zone. The labeling of

TABLE III. Table of reciprocal-lattice vectors, which are involved in the evaluation of the Green's function in layer-orbital representation defined on the reconstructed surface unit cell.

$\tilde{\vec{q}}$ domain	1	2	3	4
A_0	g_r^0, A_0		g_r^1, A_1	g_r^3, A_1'
B_0	g_r^0, B_0	g_r^2, B_0'	g_r^1, B_1	g_r^3, B_1'
C_0	g_r^0, C_0	g_r^4, C_0'	g_r^1, C_1	g_r^3, C_1'
D_0	g_r^0, D_0	g_r^2, D_0'	g_r^1, D_1	g_r^5, D_1'
E_0	g_r^0, E_0	g_r^4, E_0'	g_r^1, E_1	g_r^8, E_1'
F_0	$g_r^0 F_0$	g_r^2, F_0'	g_r^3, F_1'	g_r^6, F_1''
G_0	g_r^0, G_0	g_r^4, G_0'	g_r^3, G_1'	g_r^7, G_1''

these regions is introduced in Fig. 13. In general, for any $\tilde{\vec{q}}$ four reciprocal-lattice vectors $\vec{g}_r^i$ contribute. Therefore, there are four columns of $\vec{g}_r^i$ vectors in Table III. Using the same bulk symmetry arguments which we have discussed above for only one particular $\tilde{\vec{q}}$ vector, it is easy to show that contributions from the first two columns in the table can always be transformed as to yield [with $\vec{g}_r^0=(0,0)$]

$$T_1(\tilde{\vec{q}})=\frac{N_2^r}{N_3}\sum_n \sum_{k_\perp\in[-2\pi/a,2\pi/a]} \frac{e^{i(\vec{\kappa}^m-\vec{\kappa}^{m'})\cdot\vec{k}_\perp}}{E^+-E_n(\tilde{\vec{q}},\vec{k}_\perp)} \times C^n_{am\epsilon}(\tilde{\vec{q}},\vec{k}_\perp)C^{n*}_{\alpha' m'\epsilon'}(\tilde{\vec{q}},\vec{k}_\perp)\ . \tag{A7}$$

Similarly the contributions corresponding to $\vec{g}_r^i$ vectors from columns 3 and 4 in Table III can be combined to yield

$$T_2(\tilde{\vec{q}})=e^{i(\vec{\sigma}_\epsilon^m-\vec{\sigma}_{\epsilon'}^{m'})\cdot\vec{g}_r^1}T_1(\tilde{\vec{q}}+\vec{g}_r^1)\ . \tag{A8}$$

The final expression then is

$$\langle\alpha,m,\epsilon;\tilde{\vec{q}}\,|\,G_b(E)\,|\,\alpha',m',\epsilon';\tilde{\vec{q}}\rangle = T_1(\tilde{\vec{q}})+T_2(\tilde{\vec{q}})\ , \tag{A9}$$

which is Eq. (32).

If one compares (A7)—(A9) with expression (18) of G_b expressed in a layer-orbital representation of the ideal 1×1 surface, one can see that

$$\langle\alpha,m,\epsilon;\tilde{\vec{q}}\,|\,G_b(E)\,|\,\alpha',m',\epsilon';\tilde{\vec{q}}\rangle = \tfrac{1}{2}\{\langle\alpha,m,\mu;\tilde{\vec{q}}\,|\,G_b(E)\,|\,\alpha',m',\mu';\tilde{\vec{q}}\rangle + e^{i(\vec{\sigma}_\epsilon^m-\vec{\sigma}_{\epsilon'}^{m'})\cdot\vec{g}_r^1}\langle\alpha,m,\mu;\tilde{\vec{q}}+\vec{g}_r^1\,|\,G_b(E)\,|\,\alpha',m',\mu';\tilde{\vec{q}}+\vec{g}_r^1\rangle\}\ , \tag{A10}$$

where the indices ϵ and μ, as well as ϵ' and μ' are chosen such that $\vec{\lambda}_\mu^m$ and $\vec{\lambda}_\epsilon^m$, respectively, describe the same atoms. The factor $\frac{1}{2}$ arises from $N_2=2N_2^r$.

The determination of the surface states of the ideal surface within the reconstructed surface unit cell representation necessitates the evaluation of the determinant $\tilde{D}(\tilde{\vec{q}},E)$ defined by Eq. (9). If the layers $m=1$ and $m=2$ are removed, $\tilde{D}(\tilde{\vec{q}},E)$ can be expressed in terms of G_b blocks obtained with the help of Eq. (A10). Defining

$$G_{ij}(\tilde{\vec{q}},E)=\langle\alpha,m=i,\mu;\tilde{\vec{q}}\,|\,G_b(E)\,|\,\alpha',m'=j,\mu';\tilde{\vec{q}}\rangle \tag{A11}$$

which are 4×4 matrices since μ and μ' take only the value 1, $\tilde{D}(\tilde{\vec{q}},E)$ may be written as

$$\tilde{D}(\tilde{\vec{q}},E)=-\det\tfrac{1}{2}\begin{bmatrix}A_1 & B\\ B^* & A_2\end{bmatrix}\ , \tag{A12}$$

where

$$A_i=\begin{bmatrix}G_{ii}(\tilde{\vec{q}})+G_{ii}(\tilde{\vec{q}}+\vec{g}_r^1))\ , & G_{ii}(\tilde{\vec{q}})-G_{ii}(\tilde{\vec{q}}+\vec{g}_r^1)\\ G_{ii}(\tilde{\vec{q}})-G_{ii}(\tilde{\vec{q}}+\vec{g}_r^1)\ , & G_{ii}(\tilde{\vec{q}})+G_{ii}(\tilde{\vec{q}}+\vec{g}_r^1)\end{bmatrix}\ , \tag{A13}$$

with $i=1,2$ and

$$B=\begin{bmatrix} G_{12}(\tilde{\vec{q}})+G_{12}(\tilde{\vec{q}}+\vec{g}_r^{\,1}) , & G_{12}(\tilde{\vec{q}})-G_{12}(\tilde{\vec{q}}+\vec{g}_r^{\,1}) \\ G_{12}(\tilde{\vec{q}})-G_{12}(\tilde{\vec{q}}+\vec{g}_r^{\,1}) , & G_{12}(\tilde{\vec{q}})+G_{12}(\tilde{\vec{q}}+\vec{g}_r^{\,1}) \end{bmatrix} . \tag{A14}$$

The phase factors $e^{i(\vec{\sigma}_\epsilon^{\,m}-\vec{\sigma}_\epsilon^{\,m'})\cdot\vec{g}_r^{\,1}}$ yield simply $+1$ or -1 for this case.

Through appropriate permutations and linear combinations of lines and columns, $\tilde{D}(\tilde{\vec{q}},E)$ can be cast into the form

$$\tilde{D}(\tilde{\vec{q}},E)=D(\tilde{\vec{q}},\vec{E})D(\tilde{\vec{q}}+\vec{g}_r^{\,1},E) , \tag{A15}$$

where $D(\tilde{\vec{q}},E)$ is given by

$$D(\tilde{\vec{q}},E)=\det\begin{bmatrix} G_{11}(\tilde{\vec{q}}) , & G_{12}(\tilde{\vec{q}}) \\ G_{21}(\tilde{\vec{q}}) , & G_{22}(\tilde{\vec{q}}) \end{bmatrix} ,$$

and similarly for $D(\tilde{\vec{q}}+\vec{g}_r^{\,1},E)$. This expresses the factorization of $\tilde{D}(\tilde{\vec{q}},E)$, as written in relation (36).

[1]J. Pollmann, in *Festkörperprobleme, Advances in Solid State Physics,* edited by J. Treusch (Vieweg, Braunschweig, 1980), Vol. XX, p. 117; J. Pollmann and S. T. Pantelides, Phys. Rev. B 18, 5524 (1978); I. Ivanov, A. Mazur, and J. Pollmann, Surf. Sci. 92, 365 (1980).

[2]M. Schlüter, in *Festkörperprobleme, Advances in Solid State Physics,* edited by J. Treusch (Vieweg, Braunschweig, 1978), Vol. XVIII, p. 155.

[3]M. Lannoo, in *The Handbook of Surfaces and Interfaces,* edited by L. Dobrzynski (Garland, New York, 1978), Vol. I.

[4]C. Calandra and G. Santoro, J. Phys. C 9, L51 (1976); C. Calandra, F. Manghi, and C. M. Bertoni, *ibid.* 10, 1911 (1977).

[5]E. J. Mele and J. D. Joannopoulos, Surf. Sci. 66, 38 (1977); Phys. Rev. B 17, 1816 (1978).

[6]D. J. Chadi, Phys. Rev. B 18, 1800 (1978); 19, 2074 (1979).

[7]S. Tougaard, Phys. Rev. B 18, 3799 (1978).

[8]J. R. Chelikowsky, S. G. Louie, and M. L. Cohen, Phys. Rev. B 14, 4724 (1976); J. R. Chelikowsky and M. L. Cohen, *ibid.* 20, 4150 (1979).

[9]A. Zunger, Phys. Rev. B 22, 959 (1980).

[10]W. A. Harrison, Surf. Sci. 55, 1 (1976).

[11]J. A. Appelbaum, G. A. Baraff, and D. R. Hamann, Phys. Rev. Lett. 35, 729 (1975); Phys. Rev. B 12, 5749 (1975); 14, 588 (1976); 15, 2408 (1977).

[12]G. P. Kerker, S. G. Louie, and M. L. Cohen, Phys. Rev. B 17, 706 (1978).

[13]D. J. Chadi, Phys. Rev. Lett. 43, 43 (1979); J. Vac. Sci. Technol. 16, 1290 (1979).

[14]J. Ihm, M. L. Cohen, and D. J. Chadi, Phys. Rev. B 21, 4592 (1980).

[15]M. Schmeits, A. Mazur, and J. Pollmann, Solid State Commun. 40, 1081 (1981).

[16]A. Mazur, J. Pollmann, and M. Schmeits, Solid State Commun. 42, 37 (1982).

[17]P. K. Larsen, J. F. van der Veen, A. Mazur, J. Pollmann, J. H. Neave, and B. A. Joyce, Phys. Rev. B 26, 3222 (1982).

[18]J. C. Slater and G. F. Koster, Phys. Rev. 94, 1498 (1954).

[19]W. A. Harrison, *Electronic Structure and the Properties of Solids* (Freeman, San Francisco, 1980).

[20]R. P. Beres, R. E. Allen, J. P. Buisson, M. A. Bowen, G. F. Blackwell, H. P. Hjalmarson, and J. D. Dow, J. Vac. Sci. Technol. 21, 548 (1982), and references therein.

[21]S. Y. Tong, A. R. Lubinsky, B. I. Mrstik, and M. A. van Hove, Phys. Rev. B 17, 3303 (1978).

[22]R. J. Meyer, C. B. Duke, A. Paton, A. Kahn, E. So, J. L. Yeh, and P. Mark, Phys. Rev. B 19, 5194 (1979); C. B. Duke, R. J. Meyer, A. Paton, P. Mark, A. Kahn, E. So, and J. L. Yeh, J. Vac. Sci. Technol. 16, 1252 (1979).

[23]D. J. Chadi, Phys. Rev. Lett. 41, 1062 (1978), and Ref. 13; K. C. Padney, *ibid.* 49, 223 (1982).

[24]T. C. Chiang, J. A. Knapp, M. Aono, and D. E. Eastman, Phys. Rev. B 21, 3513 (1980).

[25]D. E. Aspnes, C. G. Olson, and D. W. Lynch, Phys. Rev. B 12, 2527 (1975).

[26]L. Ley, R. A. Pollak, F. R. McFeely, S. P. Kowalczyk, and D. A Shirely, Phys. Rev. B 9, 600 (1974).

[27]D. A. Papaconstantopoulos and E. N. Economou, Phys. Rev. B 22, 2903 (1980).

[28]An alternative approach for an improved description of the conduction bands has been to take into account an empty s^* orbital; see, e.g., H. P. Hjalmarson, P. Vogl, D. J. Wolford, and J. D. Dow, Phys. Rev. Lett. 44, 810 (1980).

[29]A. Huijser, J. van Laar, and T. L. van Rooy, Phys. Lett. 65A, 377 (1978).

[30]G. P. Williams, R. J. Smith, and G. P. Lapeyre, J. Vac.

Sci. Technol. 15, 1249 (1978).
[31]J. A. Knapp, D. E. Eastman, K. C. Pandey, and F. Patella, J. Vac. Sci. Technol. 15, 1252 (1978).
[32]F. S. Kamkalow and M. Skibowski (unpublished).
[33]V. Dose, H. J. Grossman, and D. Straub, Phys. Rev. Lett. 47, 608 (1981).
[34]W. Gudat and D. E. Eastman, J. Vac. Sci. Technol. 13, 831 (1976).
[35]F. Jona, H. D. Shih, D. W. Jepsen, and P. M. Marcus, J. Phys. C 12, L455 (1975), and references herein; see also W. S. Yang, F. Jona, and P. M. Marcus, Solid State Commun. 43, 847 (1982).
[36]M. I. Cardillo and G. E. Becker, Phys. Rev. B 21, 1497 (1980).
[37]R. E. Schlier and H. E. Farnsworth, J. Chem. Phys. 30, 917 (1950).
[38]R. Seiwatz, Surf. Sci. 2, 473 (1964); F. Jona *et al.*, J. Phys. C 10, L67 (1977).
[39]See Ref. 37 and J. A. Appelbaum and D. R. Hamann, Surf. Sci. 74, 21 (1978).
[40]M. T. Yin and M. L. Cohen, Phys. Rev. B 24, 2303 (1981).
[41]F. J. Himpsel and D. E. Eastman, J. Vac. Sci. Technol. 16, 1297 (1979).
[42]D. E. Eastman, J. Vac. Sci. Technol. 17, 492 (1980).
[43]R. M. Tromp, R. G. Smenk, and F. W. Saris, Phys. Rev. Lett. 46, 939 (1981); see also M. Aono *et al.*, *ibid.* 49, 567 (1982).
[44]F. J. Himpsel, P. Heimann, T. C.-Chiang, and D. E. Eastman, Phys. Rev. Lett. 45, 1112 (1980).
[45]A. Redondo and W. A. Goddard III, J. Vac. Sci. Technol. 21, 344 (1982).
[46]K. C. Pandey and J. C. Phillips, Phys. Rev. B 13, 750 (1976).
[47]H. A. van Hoof and M. J. van der Wiel, Appl. Surf. Sci. 6, 444 (1980).
[48]R. I. G. Uhrberg, G. V. Hansson, J. M. Nicholls, and S. A. Flodström, Phys. Rev. B 24, 4684 (1981).
[49]A more detailed comparison of our results with the theoretical results of Refs. 13 and 14 and the experimental results of Refs. 41, 47, and 48 is given by A. Mazur and J. Pollmann, Phys. Rev. B 26, 7086 (1982).